

# Computational comparison of the kinetic stabilities of diamino- and diamidocarbenes in the 1,2-H shift reaction

Chin-Hung Lai

Received: 11 January 2013 / Accepted: 5 March 2013 / Published online: 5 April 2013  
© Springer-Verlag Berlin Heidelberg 2013

**Abstract** In this study, we performed several DFT, MP2, and BD(T) calculations on the 1,2-H shift reactions of two diaminocarbenes (**1**, **2**) and a diamidocarbene (**3**) using the Gaussian 09 program. In Gaussian 09, the BD(T) method keyword requests a Brueckner doubles calculation including a perturbative triples contribution. Although *N*-heterocyclic carbenes (NHC) are typically known for their exceptional  $\sigma$ -donor abilities, recent studies have indicated that  $\pi$ -interactions also play a role in the bonding between NHCs and transition metals or  $BX_3$  ( $X = H, OH, NH_2, CH_3, CN, NC, F, Cl, \text{ and } Br$ ) (Nemesok et al. *Organomet* 23:3640–3646, 2004, Esrafilii. *J Mol Model* 18:2003–2011, 2012). In order to study the importance of  $\pi$ -interactions between carbenes and transition metals, Hobbs and co-workers (Hobbs et al. *New J Chem* 34:1295–1308, 2010) focused on the synthesis of NHCs with reduced-energy lowest unoccupied molecular orbitals. By introducing an oxalamide moiety into the heterocyclic backbone, they found the resulting carbene possessed higher electrophilicity than usual NHCs. According to our results, the *N,N'*-diamidocarbene should be more stable than the diaminocarbenes with respect to the 1,2-H shift reaction.

**Keywords** DFT · Diamidocarbene · 1,2-H shift reaction · Oxalamide

## Introduction

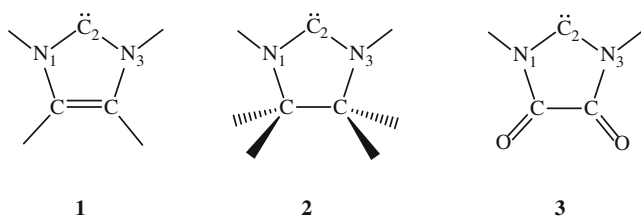
Carbenes are neutral compounds that contain divalent carbons with only six electrons in their valence shells [1]. Carbenes are commonly generated from diazoalkanes ( $R_2C = N = N$ ) via

photolytic, thermal, or transition metal-catalyzed processes [2]. For many years, carbenes were thought of only as transient species. However, in 1991, Arduengo and coworkers successfully isolated a nucleophilic carbene, structurally represented by **1** (Scheme 1) [3]. The X-ray structure of their compound revealed that the N–C bond lengths in the ring of the *N*-heterocyclic carbene (NHC) were shorter than those in the parent imidazolium compound, indicating that the N–C bonds had very little double bond character [3]. Since then, various quantum chemical calculations have been performed to investigate the peculiar stability of these Arduengo-type NHC carbenes [4–9]. The results showed that cyclic delocalization and/or resonance ( $6\pi e^-$ ) in the imidazole ring were not dominant factors in their stabilization [4–9]. Indeed, in 1995, Arduengo and coworkers successfully synthesized the corresponding saturated carbene, **2** (Scheme 1) [10].

NHCs have played vital roles in a variety of chemical reactions [11]. For example, stable NHCs have become an important class of ligands in homogeneous catalysis [11, 12]. This is due to the fact that the  $\sigma$ -symmetric lone pair on the carbenic carbon allows NHCs to form strong  $\sigma$ -coordination bonds with transition metals. Although they are typically known for their exceptional  $\sigma$ -donor abilities [13], recent studies have indicated that  $\pi$ -interactions also play a role in the bonding between NHCs and transition metals [14–19]. This  $\pi$ -interaction involving NHCs is present not only in transition metal complexes, but also in Lewis acid–base pairs such as imidazol-2-ylidene– $BX_3$  ( $X = H, OH, NH_2, CH_3, CN, NC, F, Cl, \text{ and } Br$ ) [20]. In order to study the importance of  $\pi$ -interactions between carbenes and transition metals, Hobbs and co-workers focused on preparing NHCs with reduced-energy lowest unoccupied molecular orbitals (LUMOs) [21]. By introducing an oxalamide into the heterocyclic backbone (e.g., **3**, Scheme 1), they found that the resulting carbene possessed higher electrophilicity than usual NHCs.

C.-H. Lai (✉)

School of Applied Chemistry and Department of Medical Education, Chung Shan Medical University,  
402, Taichung, Taiwan  
e-mail: chlai125@csmu.edu.tw



**Scheme 1** Structural representations of diamino- and diamidocarbenes **1**, **2**, and **3**

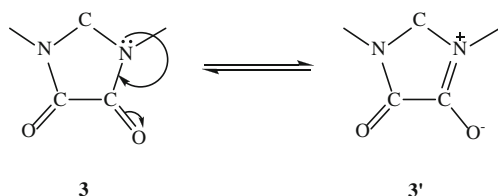
In NHCs, the filled nitrogen 2p orbitals interact strongly with the unoccupied carbon 2p orbital. However, with the insertion of the oxalamide fragment into the heterocyclic backbone, new resonance structures reduce such orbital interactions. The resonance in **3** can be represented as shown in Scheme 2. Owing to this difference, the presence of the oxalamide moiety in the heterocyclic backbone should exert additional influence on the heterocyclic carbene other than on its electrophilicity.

In this study, our goal was to investigate the difference in the relative kinetic stabilities of singlet-state *N*-heterocyclic carbenes with respect to singlet-state *N,N'*-diamidocarbenes. The 1,2-H shift reactions shown in Scheme 3 were chosen as prototypes for these comparisons. The higher the barrier, the greater the stability of the carbene. Carbene **4** (Scheme 4) was also considered to ensure a more systematic comparison.

### Theoretical aspects

All calculations were performed using the Gaussian 09 program [22]. The second-order many-body perturbation method (MP2), six hybrid generalized gradient approximation density functional theory (GGA DFT) functionals (B3LYP, B3P86, B3PW91, MPW1LYP, MPW1PW91, and MPW1K), and six hybrid meta-GGA DFT functionals (TPSSH, M05, M05-2X, M06-HF, M06, and M06-2X) were chosen and combined with the correlation-consistent triple- $\xi$  basis set, cc-pVTZ [23–35]. The difference between a hybrid GGA DFT functional and a hybrid meta-GGA DFT functional is whether the up and down spin kinetic energy densities are neglected.

All three points of interest, including reactants, transition states (TS), and products, on the potential energy surfaces (PES) of the isomerization reactions were investigated. All



**Scheme 2** Resonance structures for **3**

stationary points were positively identified as equilibrium structures (numbers of imaginary frequency (NIMAG=0)) or transition states (NIMAG=1). For the transition states, motions corresponding to the imaginary frequency were checked visually. All mentioned energetic values were corrected for zero point energies (ZPE). To obtain more accurate energetic values, single-point energy calculations were also performed at the BD(T)/cc-pVQZ//MP2/cc-pVTZ plus the MP2-optimized zero-point vibrational energies [hereafter designated as BD(T)] [36]. The most accurate wavefunction which is possible to construct for a given basis is full CI (FCI), which includes all excitations. Brueckner orbitals are defined to be those orbitals for which the coefficients of the single replacement determinants  $\phi_i^a$  in the FCI expansion are zero [37]. In Gaussian 09, the BD(T) method keyword requests a Brueckner doubles calculation including a perturbative triples contribution. The MP2 and BD(T) calculations in this study did not include core electron excitations, to conserve computational resources. This simplification was acceptable because the core electrons are more inert than the valence electrons; this approach has been adopted in related studies [38]. For the BD(T) method, the core orbitals were updated to conform to the condition T1=0 during the computing procedure.

Natural bond orbital (NBO) analysis was performed using NBO 5.9, implemented in Gaussian 09 [39]. NBOs represent orthonormal sets of localized “maximum occupancy” orbitals that describe the molecular bonding pattern of electron pairs to yield the most accurate Lewis-like description of the total N-electron density.

### Results and discussion

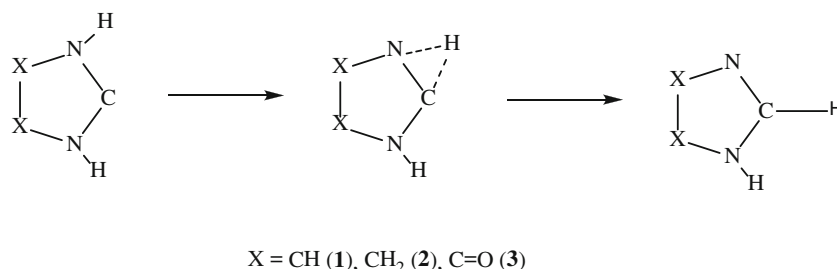
#### The most suitable DFT functional

The accuracies of the chosen DFT functionals were investigated by the relative errors of the calculated barriers ( $E_a$ ) and heats ( $\Delta H_r$ ) of the isomerization of **1** (Scheme 2) with respect to those of BD(T). The values calculated by the chosen methods are summarized in Table 1. For comparative purposes, previously published results are also summarized in the table [40].

As the calculated barrier of a DFT functional shows less deviation from that of BD(T), it can be said that the DFT functional has a higher accuracy. Therefore, two relative errors ( $\Delta E1$  and  $\Delta E2$ ) were introduced as Eqs. (1) and (2):

$$\Delta E1 = \frac{|E_a(X) - E_a[BD(T)]|}{|E_a[BD(T)]|} \quad (1)$$

$$\Delta E2 = \frac{|\Delta H(X) - \Delta H[BD(T)]|}{|\Delta H[BD(T)]|}, \quad (2)$$

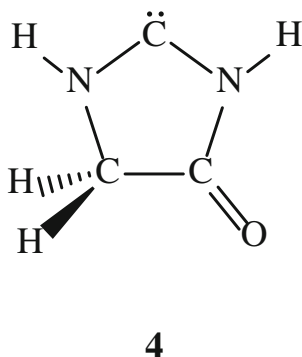
**Scheme 3** The 1,2-H shift reactions of **1**, **2**, and **3**

where X represents the selected DFT functionals and MP2. The errors for the chosen methods in this study are also summarized in Table 1. As can be seen, the chosen correlation functional had an influence on the  $E_a$  and  $\Delta H_r$  of the isomerization of **1**. For example, both  $\Delta E1$  and  $\Delta E2$  of B3LYP were less than those of B3P86. Also, the hybridization parameters of the hybrid DFT functional influenced the  $E_a$  and  $\Delta H_r$  values. For example, the MPW1K functional can be viewed as a reparameterized MPW1PW91 functional [29].  $\Delta E1$  increased from 1.72 to 4.35 % as the chosen functional was changed from MPW1PW91 to MPW1K. In contrast,  $\Delta E2$  decreased from 2.16 to 0.585 % as the MPW1PW91 was changed to the MPW1K functional. The recent B3LYP results, which were different from the previously reported B3LYP results, may be ascribed to the difference in the basis sets [40].

To find a suitable DFT functional for further study, the average relative error ( $\Delta E_{av}$ ) was introduced, as given by Eq. (3). A lower ADE value indicates a higher reliability of the DFT functional results.

$$\Delta E_{av} = \frac{\Delta E1 + \Delta E2}{2} \quad (3)$$

The  $\Delta E_{av}$ s of the chosen methods in this study are also listed in Table 1. As shown, the hybrid meta-GGA functional, M06-2X, had the smallest  $\Delta E_{av}$  among the chosen methods. Therefore, the following investigation was mainly based on the M06-2X/cc-pVTZ theoretical level.

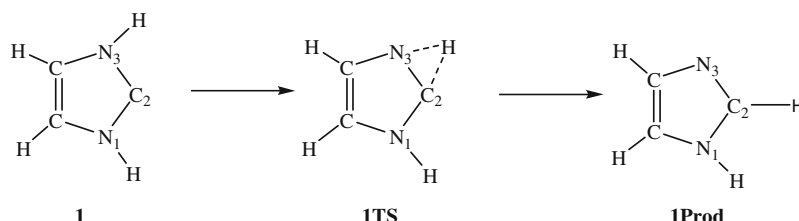
**Scheme 4** Structural representation of carbene **4**

The converged geometries of **1**, **1TS** (the transition state of the isomerization reaction), and **1Prod** (the 1,2-H shift isomer of **1**) are depicted in Fig. 1. As shown, our M06-2X results predicted a later transition state for the 1,2-H shift reaction of **1** than the previous B3LYP calculations. According to Hammond's postulate, a later transition state corresponds to a larger barrier height and lower exothermicity [41]. Indeed, as indicated in Table 1, the M06-2X/cc-pVTZ theoretical level predicted a higher barrier by 4.2 kcal mol<sup>-1</sup> than the B3LYP/6-31G\* calculations, and the exothermicity of the 1,2-H shift reaction of **1** was lower by 4.7 kcal mol<sup>-1</sup>, based on the M06-2X/cc-pVTZ theoretical level. Advanced inspection of Fig. 1 shows that **1** has C<sub>2v</sub> symmetry. Such an isomerization reaction may be driven by the formation of a stronger C-H bond (99.4 kcal mol<sup>-1</sup>) from a weaker N-H bond (93.5 kcal mol<sup>-1</sup>) [42]. However, **1Prod** possesses lower symmetry due to the difference in the lengths of its two C-N bonds.

Natural bond orbital (NBO) analyses were performed to investigate the electronic properties of **1** and **1Prod**. These results are summarized in Table 2. The bond orders listed in Table 2 are based on the Wiberg bond index matrix in the natural atomic orbital (NAO) basis [43]. Inspection of Table 2 indicates that the bond order between nitrogen and the original carbenic carbon increased once the 1,2-H shift reaction occurred. At the same time, the bond order between the other nitrogen and the carbenic carbon decreased from 1.286 to 1.212. All the mentioned lone pairs were mainly hybridized by the s and p orbitals of carbon or nitrogen. In contrast, the d orbitals seemed to have no contribution to the lone pair of the carbenic carbon or nitrogen.

The isomerization reactions of **1**, **2**, **3**, and **4**

According to the comparisons above, the M06-2X functional was chosen to study the 1,2-H shift reactions for **2–4**. The transition states (TS) corresponding to the isomerization reactions of **2**, **3**, and **4** are depicted in Fig. 2. Notably, **4** possessed both amido- and amino-type nitrogens. Therefore, **4** exhibited two transition states for the 1,2-H shift. For easier comparison, the previous results for **2TS** are also summarized in Fig. 2 [40]. Similarly, the M06-2X/cc-pVTZ theoretical level predicted a later transition state for **2** than

**Table 1**  $E_a$ ,  $\Delta H_r$  (both in kcal mol<sup>-1</sup>),  $\Delta E1$ , and  $\Delta E2$  for the isomerization of **1**


	$E_a$	$\Delta H_r$	$\Delta E1$	$\Delta E2$	$\Delta E_{av}$
B3LYP	41.6	-26.4	1.37 %	1.23%	0.685%
B3P86	40.5	-26.6	2.70%	1.91%	2.30%
B3PW91	40.4	-26.8	2.96%	2.48%	2.72%
MPW1LYP	42.4	-26.2	1.73%	0.457%	1.09%
MPW1PW91	40.9	-26.7	1.72%	2.16%	1.94%
MPW1K	43.5	-26.3	4.35%	0.585%	2.47%
TPSSH	40.0	-27.0	3.92%	3.38%	3.65%
M05	37.7	-27.0	9.51%	3.33%	6.42%
M05-2X	42.8	-26.6	2.84%	1.73%	2.28%
M06-HF	45.5	-24.5	9.21%	6.18%	7.70%
M06	39.8	-26.1	4.56%	0.0630%	2.31%
M06-2X	41.5	-25.9	0.343%	0.995%	0.669%
MP2	39.3	-29.7	5.70%	13.8%	9.75%
Previous	37.3a	-30.5a	10.4%	16.8%	13.6%
BD(T)	41.7	-26.1			

<sup>a</sup> The ZPVE-corrected results of  $E_a$  and  $\Delta H_r$  from ref. [40]

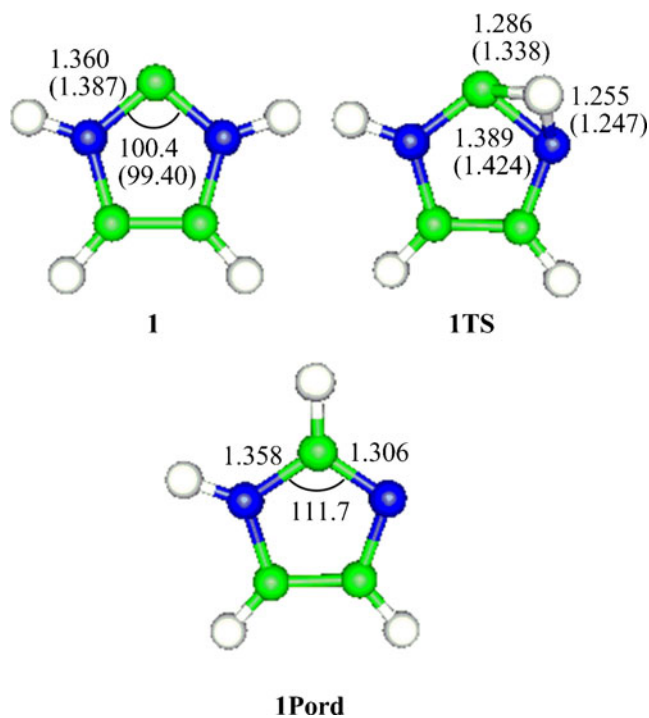


**Fig. 1** M06-2X-optimized geometric parameters for **1**, **1TS**, and **1Prod**. Bond lengths are given in Å and bond angles, in degrees. Parenthetical B3LYP values were previously reported in ref. [40]

the B3LYP/6-31G\* theoretical level. The barrier heights and the heats of reaction with respect to the chosen carbenes in this study are listed in Table 3.

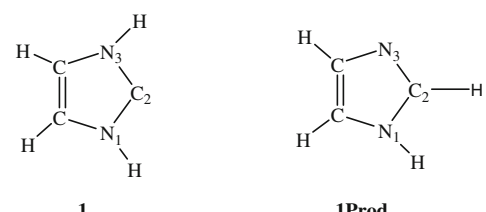
As listed in Table 3, **3** must overcome the largest activation energy to undergo a 1,2-H shift reaction. Both the results of the M06-2X/cc-pVTZ calculations and those at the B3LYP/6-31G\* theoretical level indicated that **2** had a larger barrier height for the 1,2-H shift reaction than **1**. Similarly, among all carbenes in this study, they were less stable than their 1,2-H shift isomers, according to the calculated heats of the isomerization reactions, all of which were negative. This may be due to the fact that the bond energy of a C-H bond is larger than that of a N-H bond [42]. To obtain a quantitative characterization of the position of the transition state on the PES, two parameters were introduced, as shown in Eqs. (4) and (5) [44–48]:

$$\chi^{\ddagger}(\text{Marcus}) = 0.5 + \frac{\Delta H_r}{8E_a} \quad (4)$$

$$\chi^{\ddagger}(\text{Miller}) = \frac{1}{2 - \left(\frac{\Delta H_r}{E_a}\right)}. \quad (5)$$

The calculated values of  $\chi^{\ddagger}(\text{Marcus})$  and  $\chi^{\ddagger}(\text{Miller})$  are also listed in Table 3.

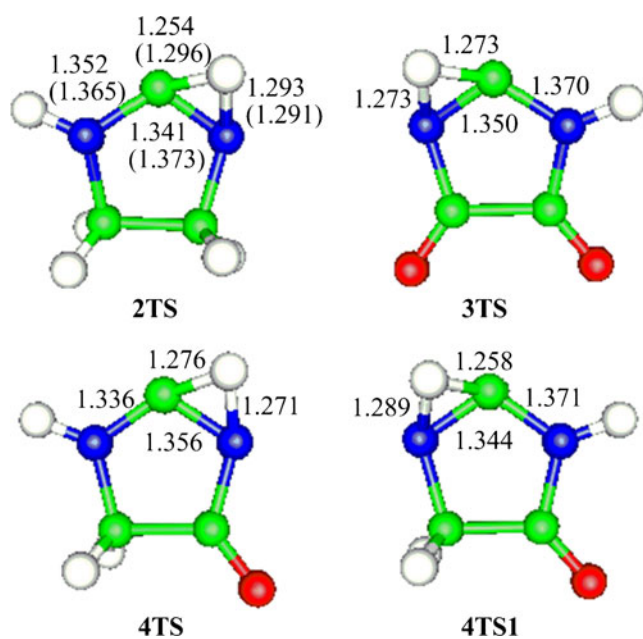
In the theory of chemical reactions, it is important to know the position of the transition state. The aforementioned

**Table 2** NBO analyses of **1** and **1Prod**


	<b>1</b>	<b>1Prod</b>
Bond order of C <sub>2</sub> -N <sub>1</sub>	1.286	1.212
Bond order of C <sub>2</sub> -N <sub>3</sub> <sup>a</sup>	1.286	1.575
Hybrids of the lone pair of C <sub>2</sub>	s:49.18% p:50.68% d:0.15% f:0.00%	–
Hybrids of the lone pair of N <sub>1</sub>	s:0.00% p:99.94% d:0.02% f:0.04%	s:0.00% p:99.95% d:0.01% f:0.04%
Hybrids of the lone pair of N <sub>3</sub> <sup>a</sup>	s:0.00% p:99.94% d:0.02% f:0.04%	s:34.75% p:64.98% d:0.26% f:0.00%

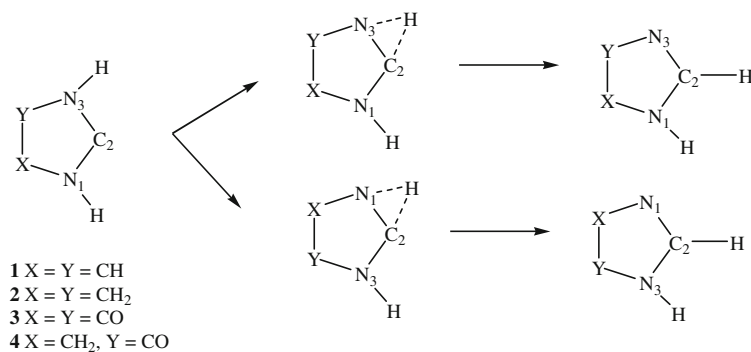
<sup>a</sup> The nitrogen atom on which the 1,2-H shift reaction occurs.

Hammond's postulate is a qualitative relationship between the transition state position and the energetics of the reaction [41]. Based on this postulate, the transition state for an endothermic reaction is product-like, whereas it is reactant-like for an



**Fig. 2** The M06-2X-optimized geometries of the transition states for **2**, **3**, and **4** (bond lengths in Å, bond angles in degrees). Parenthetical B3LYP values were previously reported in ref. [40]

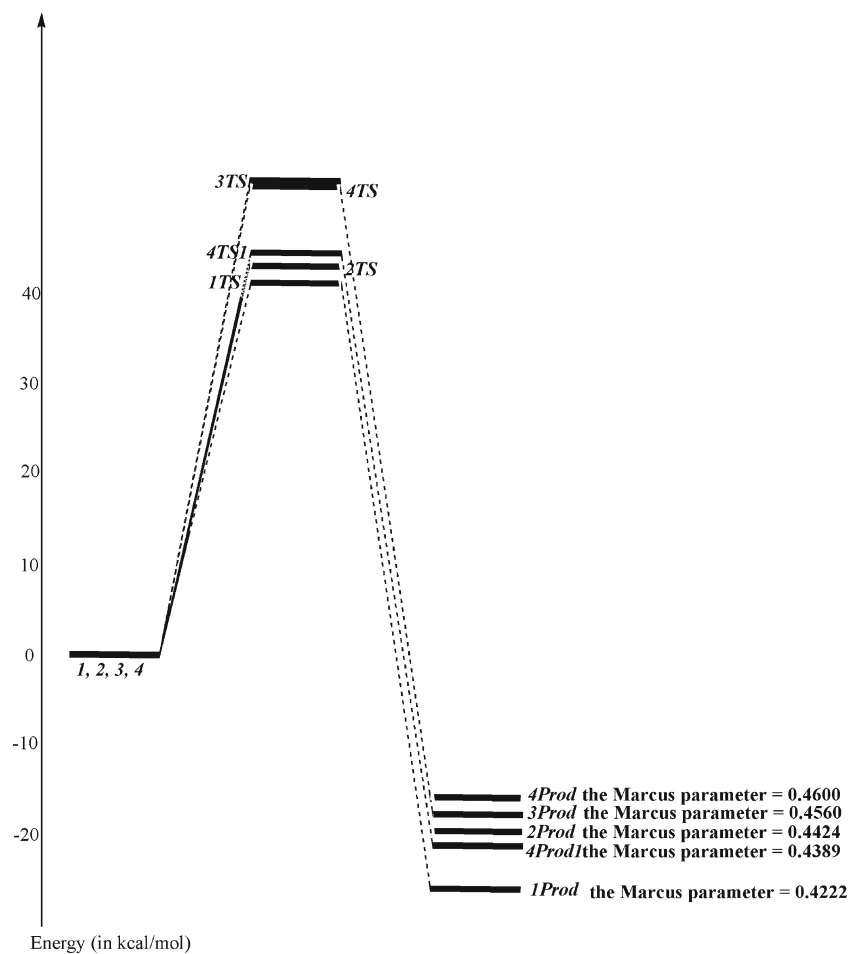
exothermic reaction. Several models have subsequently been developed to quantitatively characterize the position of the transition state. In 1968, Marcus suggested an expression for the position of the transition state ( $\chi^\ddagger$ ) that can be represented as Eq. (4) [44]. Although this equation was originally proposed for electron-transfer reactions, Murdoch and others pointed out that Eq. (4) could also be applied to other kinds of reactions [47, 48]. In 1984, Miller devised another formalism to describe the relationship between the transition state position and the energetics of the chemical reaction (Eq. (5)) [45]. Both the Marcus and Miller parameters indicate that the transition state is closer to the reactant (product) as the value of  $\chi^\ddagger$  is smaller (larger). The values of the Marcus and Miller parameters are both within 0 and 1, i.e.,  $0 \leq \chi^\ddagger(\text{Marcus}), \chi^\ddagger(\text{Miller}) \leq 1$ . The limitation values, 0 and 1, indicate the reactants and products, respectively. As listed in Table 3, the calculated values for the Marcus and Miller parameters were  $< 0.5$ , which indicates that the 1,2-H shift transition states for these carbenes are all reactant-like. A closer inspection of Table 3 shows that the previous B3LYP results gave earlier transition states for **1** and **2** [40]. Among the studied carbenes, all must overcome large barriers to undergo 1,2-H shift reactions. This may be in agreement with the well-known evidence that the stabilities of *N*-heterocyclic carbenes do not depend on substituent-migrating reactions, but rather on their

**Table 3** Barriers ( $E_a$ ), and reaction enthalpies ( $\Delta H_r$ ) for the 1,2-H shift reactions (in kcal mol<sup>-1</sup>) of **1**, **2**, **3**, and **4**

	$E_a$	$\Delta H_r$	$\chi^\ddagger$ (Marcus)	$\chi^\ddagger$ (Miller)
<b>1</b>	41.5 37.3 <sup>a</sup>	-25.8 -30.5 <sup>a</sup>	0.4222 <i>0.3978<sup>a</sup></i>	0.3813 <i>0.3549<sup>a</sup></i>
<b>2</b>	43.1 37.9 <sup>a</sup>	-19.9 -25.4 <sup>a</sup>	0.4424 <i>0.4162<sup>a</sup></i>	0.4063 <i>0.3745<sup>a</sup></i>
<b>3</b>	52.8	-18.6	0.4560	0.4251
<b>4</b>	52.5 44.8 <sup>b</sup>	-16.8 -21.9 <sup>b</sup>	0.4600 0.4389 <sup>b</sup>	0.4310 0.4018 <sup>b</sup>

<sup>a</sup> The values in italics are the previously reported B3LYP/6-31G\* results from ref. [40]

<sup>b</sup> The results for the 1,2-H shift reaction on N<sub>1</sub> in **4**

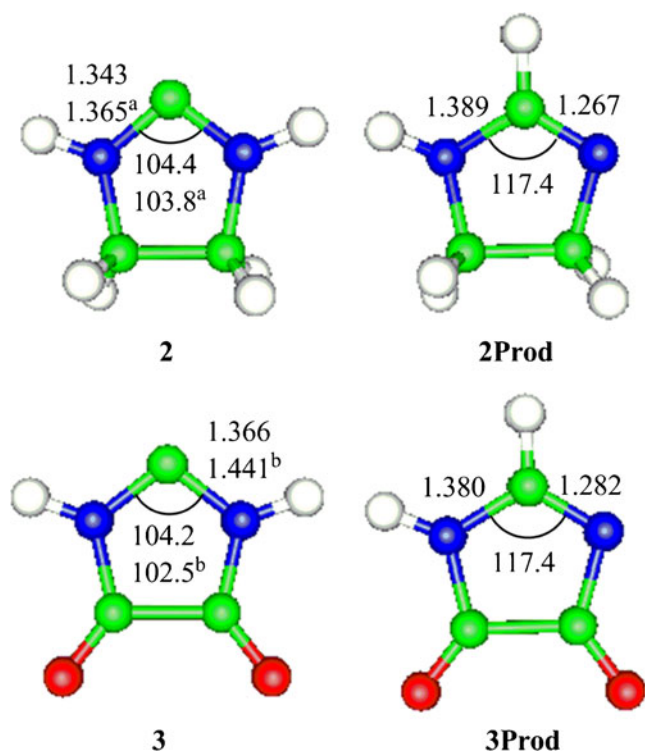
**Fig. 3** Reaction energy profiles and Marcus parameters for the 1,2-H shift reactions of **1–4**



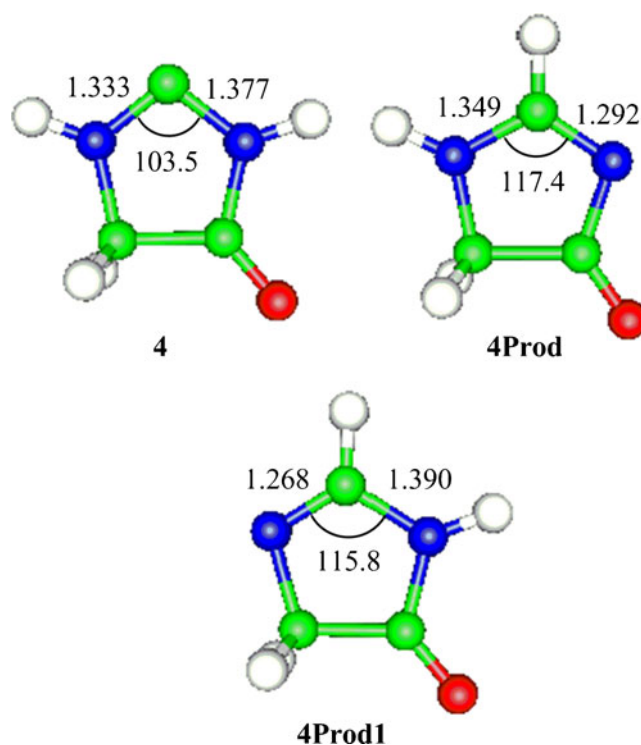
dimerization [8, 40, 49]. The reaction profiles and the calculated Marcus parameters for the 1,2-H shift reactions of **1–4** are depicted in Fig. 3. According to our results, the insertion of the oxalamide fragment did not decrease the stability of the heterocyclic carbene containing nitrogen with respect to the 1,2-H shift reaction. Indeed, the stability even increased.

For a more systematic study, the comparison was not only performed on the corresponding transition states but also on the reactants (**2**, **3**, and **4**) and the products (**2Prod**, **3Prod**, **4Prod**, and **4Prod1**). The M06-2X converged geometries were compared first. The optimized geometries of **2**, **3**, and their corresponding products (**2Prod**, **3Prod**) are summarized in Fig. 4. To facilitate comparison, the previously reported B3LYP results for **2** are also listed in Fig. 4. For systematic comparison, the optimized geometries of **4** and its corresponding products (**4Prod** and **4Prod1**) are depicted in Fig. 5.

As depicted in Fig. 4, the B3LYP/6-31G\* theoretical level gave a longer C<sub>2</sub>-N<sub>1</sub> bond length and a smaller ∠N<sub>1</sub>-C<sub>2</sub>-N<sub>5</sub> bond angle for **2** than did the M06-2X/cc-pVTZ theoretical level. The optimized geometry of **3** was different from that determined experimentally by X-ray structural analysis for the potential *N*-heterocyclic carbene precursor,



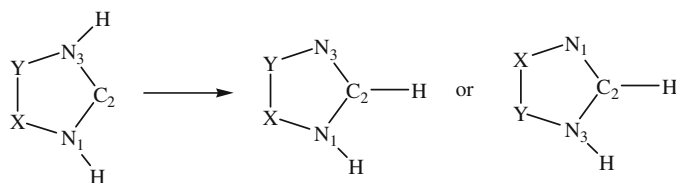
**Fig. 4** DFT-converged geometries of **2**, **3**, and their corresponding 1,2-H shift products (**2Prod**, **3Prod**). Bond lengths are given in Å, and the angles, in degrees. <sup>a</sup>Previously reported B3LYP values from ref. [40]. <sup>b</sup>X-ray structural analysis data for 1b from ref. [21]



**Fig. 5** DFT-converged geometries of **4** and its corresponding 1,2-H shift products (**4Prod**, **4Prod1**). Bond lengths are given in Å, and the angles, in degrees

2-chloro-1,3-bis(2,6-dimethylphenyl)imidazolidine-4,5-dione [21]. As depicted in Fig. 3, the bond length of C<sub>2</sub>-N<sub>1</sub>(amido) in **3** was longer than that of C<sub>2</sub>-N<sub>1</sub>(amino) in **2**. This can be rationalized by the reduction of the strong interaction between the filled nitrogen 2p orbitals with the unoccupied carbenic 2p orbital by the resonance between N(amido) and the carbonyl group. A similar situation can be seen by comparing the two C-N bond lengths in **4** (Fig. 5). As depicted in Figs. 1, 4, and 5, the 1,2-H shift reactions for all studied carbenes were accompanied by a shortening of the C<sub>2</sub>-N<sub>3</sub> bond length. For example, the C<sub>2</sub>-N<sub>3</sub> bond length of **1** decreased from 1.360 to 1.306 Å as the 1,2-H shift reaction occurred.

Next, the electric properties of the carbenes and corresponding products in this study were compared. The NBO analyses were performed on **2**, **3**, **4**, and their 1,2-H shift isomers, and the results are summarized in Table 4. As shown, the bond order of the C<sub>2</sub>-N<sub>1</sub>(amido) bond was smaller than that of the C<sub>2</sub>-N<sub>1</sub>(amino) bond. For example, the bond order of C<sub>2</sub>-N<sub>1</sub>(amido) was 1.214 in **3**. However, the bond order of C<sub>2</sub>-N<sub>1</sub>(amino) was calculated to be 1.315 in **2**. This was due to the smaller interaction between the filled nitrogen 2p orbitals with the unoccupied carbon 2p orbital in **3** than in **2**. The comparison of the bond orders of the two C-N bonds in **4** also showed the same trend. Similarly, the lone pair of C or N was mainly hybridized by the s and p orbitals of C or N.

**Table 4** NBO analyses of **2**, **3**, **4**, and their 1,2-H shift isomers

- 1** X = Y = CH  
**2** X = Y = CH<sub>2</sub>  
**3** X = Y = CO  
**4** X = CH<sub>2</sub>, Y = CO

	Bond order of C-N	Hybrids of the lone pair of C <sub>2</sub>
<b>2</b>	1.315	s:45.30% p:54.53% d:0.17% f:0.00%
<b>2Prod</b>	1.106 1.820 <sup>a</sup>	–
<b>3</b>	1.214	s:49.42% p:50.38% d:0.21% f:0.00%
<b>3Prod</b>	1.113 1.710 <sup>a</sup>	–
<b>4</b>	1.160 <sup>b</sup> 1.385 <sup>c</sup>	s:47.74% p:52.08% d:0.18% f:0.00%
<b>4Prod</b>	1.616 <sup>b</sup> 1.235 <sup>c</sup>	–
<b>4Prod1</b>	1.073 <sup>b</sup> 1.833 <sup>c</sup>	–

<sup>a</sup> The nitrogen atom on which the 1,2-H shift reaction occurred

<sup>b</sup> N<sub>3</sub> in **4**

<sup>c</sup> N<sub>1</sub> in **4**

## Conclusions

In summary, the following conclusions can be drawn from the calculations on the 1,2-H shift reactions of the carbenes depicted in Schemes 1 and 4:

- (1). Among the chosen DFT functionals and MP2 methods, M06-2X produced the smallest  $\Delta E1$  and  $\Delta E2$  with respect to BD(T).
- (2). According to the results of the M06-2X functional, the insertion of the oxalamide fragment did not destabilize the *N*-heterocyclic carbene with respect to the 1,2-H shift reaction.
- (3). Because of the resonance between the N(amido) and the C = O group, the interaction between the filled nitrogen 2p orbitals with the unoccupied carbenic 2p orbital was weakened. Therefore, the bond order of the C-N bond was calculated to be smaller in **3** than in **2**.

*N,N'*-diamidocarbenes have shown significant synthetic utility [51–53]. For example, Lee et al. found that *N,N'*-diamidocarbenes were ambiphilic, and could behave as good electrophiles and good nucleophiles [50]. We believe

that our results could provide information to better rationalize the reactivity of *N,N'*-diamidocarbenes.

**Acknowledgments** The author is grateful to the National Center for High-Performance Computing, Taiwan, for providing a generous amount of computing time. The author also thanks the National Science Council of Taiwan for financial support.

## References

1. Geuther A, Hermann M (1855) Ueber die bei der technischen gewinnung des broms beobachtete flüchtige bromverbindung. Liebigs Ann Chem 95:211–225
2. Staudinger H, Kupfer O (1912) Über reaktionen des methylen. III. Diazomethan. Ber 45:501–509
3. Arduengo AJ III, Harlow RL, Kline M (1991) A stable crystalline carbene. J Am Chem Soc 113:361–363
4. Dixon DA, Arduengo AJ III (1991) Electronic structure of a stable nucleophilic carbene. J Phys Chem 95:4180–4182
5. Arduengo AJ III, Dias HVR, Dixon DA, Harlow RL, Klooster WT, Koetzle TF (1994) Electron distribution in a stable carbene. J Am Chem Soc 116:6812–6822
6. Arduengo AJ III, Bock H, Chen H, Denk M, Dixon DA, Green JC, Herrmann WA, Jones NJ, Wagner M, West R (1994) Photoelectron



- spectroscopy of a carbene/silylene/germylene series. *J Am Chem Soc* 116:6641–6649
7. Arduengo AJ III, Dixon DA, Kumashiro KK, Lee C, Power WP, Zilm KW (1994) Chemical shielding tensor of a carbene. *J Am Chem Soc* 116:6361–6367
  8. Heinemann C, Thiel W (1994) Ab initio study on the stability of diaminocarbenes. *Chem Phys Lett* 217:11–16
  9. Heinemann C, Müller T, Apeloig Y, Schwarz H (1996) On the question of stability, conjugation, and “aromaticity” in imidazol-2-ylidenes and their silicon analogs. *J Am Chem Soc* 118:2023–2028
  10. Arduengo AJ III, Goerlich JR, Marshall WJ (1995) A stable diaminocarbene. *J Am Chem Soc* 117:11027–11028
  11. Enders D, Balensiefer T (2004) Nucleophilic carbenes in asymmetric organocatalysis. *Acc Chem Res* 37:534–541
  12. Herrmann WA, Weskamp T, Böhm VPW (2002) Metal complexes of stable carbenes. *Adv Organomet Chem* 48:1–69
  13. Huang J, Schanz H-J, Stevens ED, Nolan SP (1999) Stereoelectronic effects characterizing nucleophilic carbene ligands bound to the Cp\*RuCl (Cp\*= $\eta^5$ -C<sub>5</sub>Me<sub>5</sub>) moiety: a structural and thermochemical investigation. *Organomet* 18:2370–2375
  14. Nemcsok D, Wichmann K, Frenking G (2004) The significance of  $\pi$  interactions in group 11 complexes with *N*-heterocyclic carbenes. *Organomet* 23:3640–3646
  15. Sanderson MD, Camplain JW, Bielawski CW (2006) Quinone-annulated *N*-heterocyclic carbene – transition metal complexes: observation of  $\pi$ -backbonding using FT-IR spectroscopy and cyclic voltammetry. *J Am Chem Soc* 128:16514–16515
  16. Diez-Gonzalez S, Nolan SP (2007) Stereoelectronic parameters associated with *N*-heterocyclic carbene (NHC) ligands: a quest for understanding. *Coord Chem Rev* 251:874–883
  17. Khranov DM, Lynch VM, Bielawski CW (2007) *N*-heterocyclic carbene – transition metal complexes: spectroscopic and crystallographic analyses of  $\pi$ -back-bonding interactions. *Organomet* 26:6042–6049
  18. Kausamo A, Tuononen HM, Krahulic KE, Roesler R (2008) *N*-heterocyclic carbenes with inorganic backbones: electronic structures and ligand properties. *Inorg Chem* 47:1145–1154
  19. Srebro M, Michalak A (2009) Theoretical analysis of bonding in *N*-heterocyclic carbene – rhodium complexes. *Inorg Chem* 48:5361–5369
  20. Esrafil MD (2012) Characteristics and nature of the intermolecular interactions in boron-bonded complexes with carbene as electron donor: an Ab initio, SAPT, and QTAIM study. *J Mol Model* 18:2003–2011
  21. Hobbs MG, Forster TD, Borau-Garcia J, Knapp C, Tuononen HM, Roesler R (2010) The influence of electron delocalization upon the stability and structure of potential *N*-heterocyclic carbene precursors with 1,3-diaryl-imidazolidine-4,5-dione skeletons. *New J Chem* 34:1295–1308
  22. Frisch MJ, Trucks GW, Schlegel HB, Scuseria GE, Robb MA, Cheeseman JR, Scalmani G, Barone V, Mennucci B, Petersson GA, Nakatsuji H, Caricato M, Li X, Hratchian HP, Izmaylov AF, Bloino J, Zheng G, Sonnenberg JL, Hada M, Ehara M, Toyota K, Fukuda R, Hasegawa J, Ishida M, Nakajima T, Honda Y, Kitao O, Nakai H, Vreven T, Montgomery, Jr JA, Peralta JE, Ogliaro F, Bearpark M, Heyd JJ, Brothers E, Kudin KN, Staroverov VN, Kobayashi R, Normand J, Raghavachari K, Rendell K, Burant JC, Iyengar SS, Tomasi J, Cossi M, Rega N, Millam JM, Klene M, Knox JE, Cross JB, Bakken V, Adamo C, Jaramillo J, Gomperts R, Stratmann RE, Yazyev O, Austin AJ, Cammi R, Pomelli C, Ochterski JW, Martin RL, Morokuma K, Zakrzewski VG, Voth GA, Salvador P, Dannenberg JJ, Dapprich S, Daniels AD, Farkas O, Foresman JB, Ortiz JV, Cioslowski J, Fox DJ (2010) Gaussian 09, revision C.01. Gaussian Inc., Wallingford, CT
  23. Head-Gordon M, Pople JA, Frisch MJ (1988) MP2 Energy evaluation by direct methods. *Chem Phys Lett* 153:503–506
  24. Becke AD (1993) Density-functional thermochemistry. III. The role of exact exchange. *J Chem Phys* 98:5648–5652
  25. Lee C, Yang W, Parr RG (1988) Development of the colle-salvetti correlation-energy formula into a functional of the electron density. *Phys Rev B* 37:785–789
  26. Perdew JP, Zunger A (1981) Self-interaction correction to density-functional approximations for many-electron systems. *Phys Rev B* 23:5048–5079
  27. Perdew JP, Chevary JA, Vosko SH, Jackson KA, Pederson MR, Singh DJ, Fiolhais C (1992) Atoms, molecules, solids, and surfaces: applications of the generalized gradient approximation for exchange and correlation. *Phys Rev B* 46:6671–6687
  28. Adamo C, Barone V (1997) Toward reliable adiabatic connection models free from adjustable parameters. *Chem Phys Lett* 274:242–250
  29. Lynch BJ, Fast PL, Harris M, Truhlar DG (2000) Adiabatic connection for kinetics. *J Phys Chem A* 104:4811–4815
  30. Staroverov VN, Scuseria GE, Tao J, Perdew JP (2003) Comparative assessment of a New nonempirical density functional: molecules and hydrogen-bonded complexes. *J Chem Phys* 119:12129–12137
  31. Zhao Y, Schultz NE, Truhlar DG (2006) Design of density functionals by combining the method of constraint satisfaction with parametrization for thermochemistry, thermochemical kinetics, and noncovalent interactions. *J Chem Theory Comput* 2:364–382
  32. Zhao Y, Truhlar DG (2006) Density functional for spectroscopy: No long-range self-interaction error, good performance for rydberg and charge-transfer states, and better performance on average than B3LYP for ground states. *J Phys Chem A* 110:13126–13130
  33. Zhao Y, Truhlar DG (2008) The M06 suite of density functionals for main group thermochemistry, thermochemical kinetics, noncovalent interactions, excited states, and transition elements: Two New functionals and systematic testing of four M06-class functionals and 12 other functionals. *Theor Chem Acc* 120:215–241
  34. Zhao Y, Truhlar DG (2008) Density functionals with broad applicability in chemistry. *Acc Chem Res* 41:157–167
  35. Kendall RA, Dunning TH Jr, Harrison RJ (1992) Electron affinities of the first-Row atoms revisited. Systematic Basis Sets and Wave Functions. *J Chem Phys* 96:6796–6806
  36. Handy NC, Pople JA, Head-Gordon M, Raghavachari K, Trucks GW (1989) Size-consistent brueckner theory limited to double substitutions. *Chem Phys Lett* 164:185–192
  37. van Heusden CM, Kobayashi R, Amos RD, Handy NC (1993) Electron densities from the brueckner doubles method. *Theor Chim Acta* 86:25–39
  38. Zhu L, Bozzelli JW (2002) Thermodynamic properties of chloroacetylene, dichloroacetylene, ethynyl radical, and chloroethynyl radical. *Chem Phys Lett* 362:445–452
  39. Foster JP, Weinhold F (1980) Natural hybrid orbitals. *J Am Chem Soc* 102:7211–7218
  40. Cheng M-J, Hu C-H (2000) A computational study on the stability of diaminocarbenes. *Chem Phys Lett* 322:83–90
  41. Hammond GS (1955) A correlation of reaction rates. *J Am Chem Soc* 77:334–338
  42. Middlecamp C, Keller SW, Anderson K, Bentley A, Cann M and Ellis J (2012) Chemistry in context: applying chemistry to society, 7th edn. McGraw-Hill, New York
  43. Wiberg KB (1968) Application of the pople-santry-segal CNDO method to the cyclopropylcarbiny and cyclobutyl cation and to bicyclobutane. *Tetrahedron* 24:1083–1096
  44. Marcus RA (1968) Theoretical relations among rate constants, barriers, and broensted slopes of chemical reactions. *J Phys Chem* 72:891–899
  45. Miller AR (1978) A theoretical relation for the position of the energy barrier between initial and final states of chemical reactions. *J Am Chem Soc* 100:1984–1992
  46. Lai C-H, Chou PT (2008) A computational study on the kinetic stability of cyclic boryl anions. *Open Chem Phys J* 1:51–61

47. Chen MY, Murdoch JR (1984) The application of marcus-like equations to processes which have no corresponding identity reactions. Separation of thermodynamic and intrinsic contributions to barriers to internal rotation and conformational rearrangements. *J Am Chem Soc* 106:4735–4743
48. Lee WT, Masel RI (1998) Ab initio tests of the marcus equation for the prediction of the position of the transition state for the reaction  $H + C_2H_5R \rightarrow CH_4 + CH_2R$  with  $R = H, CH_3, NH_2, CN, CF_3,$  and  $C_6H_5$ . *J Phys Chem A* 102:2332–2341
49. Cheng MJ, Hu CH (2001) Computational study on the stability of imidazol-2-ylidenes and imidazolin-2-ylidenes. *Chem Phys Lett* 349:477–482
50. Lee Y-G, Moerdyk JP, Bielawski CW (2012) Exploring the nucleophilicity of N, N'-diamidocarbenes: heteroallenes and related compounds as coupling reagents. *J Phys Org Chem* 25:1027–1032
51. Moerdyk JP, Bielawski CW (2012) Alkyne and reversible nitrile activation: N, N'-diamidocarbene-facilitated synthesis of cyclopropenes, cyclopropanones, and azirines. *J Am Chem Soc* 134:6116–6119
52. Moerdyk JP, Bielawski CW (2012) Diamidocarbenes as versatile and reversible [2+1] cycloaddition reagents. *Nat Chem* 4:275–280
53. Hudnall TW, Moerdyk JP, Bielawski CW (2010) Ammonia N-H activation by a N, N'-diamidocarbene. *Chem Commun* 46:4288–4290